

Contents lists available at ScienceDirect

Carbon

journal homepage: www.elsevier.com/locate/carbon



Self-organization of amorphous Q-carbon and Q-BN nanoballs

J. Narayan *, N. Khosla

Department of Materials Science and Engineering, North Carolina State University, Raleigh, NC, 27695-7907, USA



ARTICLE INFO

Article history:
Received 21 December 2021
Received in revised form
14 February 2022
Accepted 1 March 2022
Available online 3 March 2022

ABSTRACT

This paper reports for the first time the formation and self-organization of amorphous Q-carbon and Q-BN nanoballs. This is accomplished by nanosecond laser melting of carbon and BN layers, respectively, in a highly undercooled state and subsequent rapid cooling at normal pressures in air. The size of these Q-carbon and Q-BN nanoballs having a uniform size can be varied from 5 to 100 nm, and self-organized along rings and strings by manipulating laser, carbon film, and substrate parameters. It is envisaged that self-organization is promoted by the undercooling and it occurs along strings and rings, which are formed by the tetrahedral alignment in <100> and <110> directions, respectively. These nanoballs were characterized by HRSEM/TEM/STEM/EELS and Raman to confirm the phase purity and bonding characteristics. The Q-carbon balls exhibit robust ferromagnetism and field emission in pure and undoped form and show highest BCS superconducting transition temperature upon doping with boron. The ferromagnetism in Q-carbon balls can be varied with size and achieve higher coercively than thin films, and these balls can be coated with drugs for targeted delivery. In view of these properties, nanoballs are expected to find novel applications ranging from targeted delivery to nanosensing and superconducting qubits.

© 2022 Elsevier Ltd. All rights reserved.

1. Introduction

Since diamond and c-BN are metastable materials at normal temperatures and pressures, their synthesis and processing require inordinately high temperatures and pressures, 5000K and 12 GPa for diamond, and 3500K and 9.5 GPa for c-BN [1]. Synthesis and processing at such extreme temperatures and pressures also require highly inert atmospheres to prevent carbon oxidation, resulting in very low yields in the form of grits, which are not usable for thin film devices. The CVD (chemical vapor deposition) is an equilibrium method, which must be combined with nonequilibrium processes, such as hot-filament and microwaves to create diamond that is metastable (nonequilibrium) phase of carbon [2-4]. This combination of equilibrium and non-equilibrium synthesis results in the formation of nonequilibrium and metastable phase of diamond mixed with equilibrium phase of graphite, where the graphitic phase is preferentially etched by atomic hydrogen to form diamond as a remaining phase. The atomic hydrogen is produced by hot filament in HFCVD and by microwaves during MPCVD. Thus, these CVD methods present significant challenges for the

formation of phase-pure and epitaxial growth of diamond, and even bigger challenges for producing phase-pure c-BN due to a lack of preferential etching of h-BN [5]. In addition, these methods require the diamond seeds for growth because of high a nucleation barrier for diamond, especially on noncarbide forming substrates. Moreover, synthesis and processing of diamond and c-BN limit the incorporation of dopants into electrically active substitutional sites close to the equilibrium thermodynamic solubility limits, which tend to be quite low. This leads to very limited concentrations of free carriers due to deep dopant energy levels. Furthermore, these CVD methods allowed only p-type doping of diamond, making formation of p-n junctions and related solid-state devices nearly impossible [5].

Nanosecond laser processing of carbon and BN layers, nanorods and nanotubes has opened a new frontier in synthesis and processing of phase-pure diamond and c-BN at normal temperatures and pressures [6–12]). In this process, undercooled carbon and BN layers are quenched rapidly to form phase-pure diamond and c-BN, respectively, through a first-order phase transformation at normal temperature and pressure. By providing appropriate substrate template, diamond and c-BN films can be grown epitaxially via domain matching epitaxy on substrates having large lattice and thermal misfits [6,7,13]. These films can be doped with p-type and n-type dopants with concentrations substantially higher than the

Corresponding author.

E-mail address: j_narayan@ncsu.edu (J. Narayan).

thermodynamic solubility limits because of kinetically driven solute trapping [8]. The optimized conditions for laser processing are guided by detailed laser-sold interaction simulations, which take into account thin film, laser and substrate variables [14]. The key variables include optical absorption (bandgap), sp³ to sp² ratio, thermal conductivity and specific heat of the film; thermal conductivity and specific heat of the substrate; and laser wavelength (photon energy), pulse duration, and energy density of the laser pulse. By increasing the undercooling, new allotropes of carbon (Qcarbon) and BN (Q-BN) are formed [6]. Previous studies have established that Q-carbon exhibits extraordinary properties, such as, RT ferromagnetism, ultra-hardness, record BCS superconductivity, enhanced field emission, and radiation resistance [8,15]. We expect some of these properties to be enhanced further in Q-carbon and Q-BN nanoballs. Our earlier studies also showed the formation of self-organized nanodiamonds along rings and strings, which grew epitaxially with the substrate even with large misfit through the of domain matching epitaxy framework [16]. These nanodiamonds were smaller in size because of the nucleation barrier in diamond, which was not present in the growth of Q-carbon balls.

In this study, we focus on the conversion of carbon and BN layers into Q-carbon and Q-BN nanoballs, respectively. Size of these nanoballs can be varied from 5 nm to 100 nm by controlling characteristics of carbon and BN thin films, and laser and substrate variables. These nanoballs can be also self-organized in the form of rings and strings, similar to our earlier work on nanodiamonds [16]. It is shown that the self-organization along strings and rings occurs, when diamond tetrahedra are aligned along <100> and <110> directions, respectively. This study provides elegant example of formation of self-organized structures of uniform size in amorphous materials and shows interesting similarities with crystalline nanodiamond structures. A remarkable property of Q-carbon is that it is ferromagnetic in pure and undoped state, and it becomes superconducting upon doping with boron. The superconducting transition temperature increases with B concentration with the current record of 55K in 25 at%B doped Q-carbon [9,10], and the transition temperature is expected to go much higher with 50 at%B in Q-carbon nanoballs. Here we focus on the ferromagnetism of Qcarbon nanoballs and discuss enhancement of other properties in nanoballs. These Q-carbon nanoballs can be used for coating drugs and their targeted delivery, in addition to nanosensing and superconducting qubits applications.

2. Experimental details

The films of amorphous carbon having thickness of 5-500 nm were deposited on (c-plane) sapphire substrates by using KrF Excimer laser with pulse duration of 25ns, wavelength of 248 nm, and energy density of 3.0Jcm⁻². Each pulse deposits approximately 0.1 nm thick amorphous carbon. The as-deposited films were treated in air with ArF laser pulses having pulse duration of 20ns, wavelength of 193 nm, and energy density varying from 0.3 Jcm⁻² to 0.8 Jcm⁻² [6]. The laser-treated films were analyzed by highresolution TEM and Raman and were found to be amorphous containing broad E_{2g} Raman peak at 1580 cm⁻¹ from which sp³ fraction was estimated to be in the range of 20-50%. Most of the films used in our experiments contained sp³ fraction around 40%. The amorphous BN films were obtained by using h-BN targets in PLD with similar deposition conditions [7]. These films were characterized by high-resolution scanning electron microscopy (HRSEM), electron backscattered diffraction (EBSD) with characteristic diamond Kikuchi patterns, high-resolution transmission electron microscopy (HRTEM), high-resolution electron-energyloss spectroscopy (HREELS), x-ray diffraction, and Raman spectroscopy. HRSEM and EBSD measurements were performed by

using FEI Verios 460L SEM and FEI Quanta 3D FEG FIB-SEM. Aberration corrected STEM-FEI Titan 80—300 and JEOL-2010 STEM/TEM were used for HREELS measurements with resolution of 0.15eV, HRTEM with point-to-point TEM resolution of 0.18 nm; and STEM-Z resolution of 0.08 nm with information limit of 0.06 nm. For magnetic measurements, EverCool Quantum Design PPMS (physical-property measurement system) with a base temperature as low as 5 K was used with magnetic fields up to 7 T.

3. Results and discussion

By melting amorphous carbon layers and rapid cooling, we can form the equilibrium phase of carbon (graphite) and nonequilibrium phases of diamond and Q-carbon by controlling the degree of undercooling before quenching. The undercooling is determined primarily by the laser variables and by the optical and thermal properties of the film and the substrate. With no undercooling, equilibrium graphite phase is formed, and at the highest undercooling of over 1000K, Q-carbon having novel physical, chemical, and mechanical properties is formed. These temperatures were estimated by using the SLIM (simulation of laser interactions with materials) computer program developed by Singh and Narayan [14].

The conversion of amorphous carbon into metastable phases of diamond and Q-carbon is illustrated by Gibbs free energy versus temperature diagram displayed in Fig. 1. The free energy of metastable diamond and Q-carbon is higher than the equilibrium phase of graphite. It should be noted that the slope of liquid carbon is larger than those of solid phases of diamond and Q-carbon due to its higher entropy. At the intersections of liquid carbon with diamond and Q-carbon, we form diamond and Q-carbon at T_D and T_Q , respectively, by quenching from the liquid phase. The difference between these temperatures and the melting point of carbon is the undercooling, which drives the first-order phase transformation. This free energy (ΔG_T) is directly proportional to the undercooling $(\Delta T_U = Tm - T_Q)$ as $\Delta G_T = -\Delta T_U$. $\Delta H_m/T_m$, where ΔH_m and T_m (constants for a given system) are enthalpy of melting and equilibrium melting point, respectively.

Our theoretical simulations have shown that the undercooling acts like applying pressure during the first-order thermodynamic phase transformation, as discussed later. Since these liquid-to-solid phase transformations are the first order, we obtain phase-pure diamond and Q-carbon. It should be pointed out that current HFCVD and PECVD methods involve solid-phase growth of preexisting diamond nuclei, which result in mixed diamond (nonequilibrium metastable) and graphitic carbon (equilibrium) phases. The primary focus of this work is on the formation of Q-carbon in the

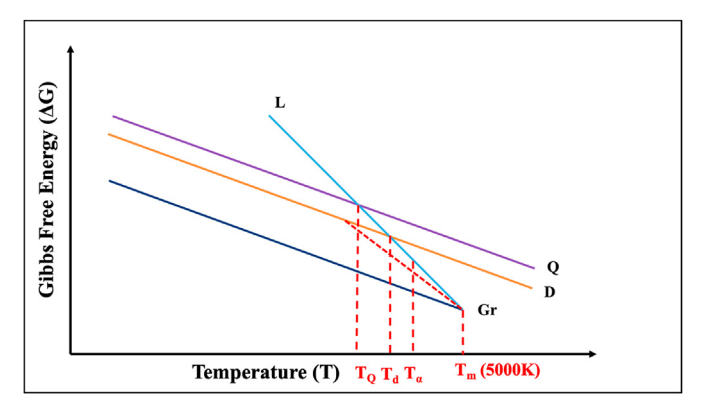


Fig. 1. Gibbs free energy (ΔG) versus temperature (T) for graphite (equilibrium phase), diamond, Q-carbon, and liquid carbon with higher entropy (slope).

form of nanoballs by quenching from T₀ (phase diagram in Fig. 1), as illustrated in Fig. 2. The amorphous nature of Q-carbon is confirmed by the selected-area electron diffraction pattern with continuous 111 and 200 diffraction rings, as shown in the inset of Fig. 2. The presence of these two rings indicates that Q-carbon structure consists of diamond tetrahedra, which are randomly packed, and the 111 and 200 faint diffraction rings correspond to first and second nearest neighbor distances. It is envisaged that Ocarbon consists of random diamond tetrahedral structure, where the bonding within the tetrahedra is sp³ and a fraction in between is sp². These nanoballs are formed by nucleation and growth of Qcarbon phase in super undercooled carbon. It is interesting to note that the nanoballs are self-organized along the strings (straight lines) and mostly (circular) rings with fairly uniform size of 50 nm. The mechanism of self-organization of Q-carbon and Q-BN balls will be discussed later. The size is determined by the growth velocity and the time available for Q-carbon growth, as the nuclei in the form of diamond tetrahedra are already present. With growth velocity of $8-10 \text{ ms}^{-1}$, and the time available for growth of 5-7 ns, the size of nanoballs is estimated to be 50 nm, which is consistent with SLIM simulation and thin-film hydrodynamic instability calculations to be discussed later. The size of Q-carbon nanoballs is much larger than self-organized nanodiamonds because of no nucleation barrier in Q-carbon [15].

Fig. 3 (a) shows HRTEM of Q-carbon, which indicates amorphous structure of Q-carbon on (120) sapphire substrate. The sp³/sp² interfaces contain dangling bonds which are responsible for ferromagnetism in nanoballs, as discussed below. To determine relative fraction of sp³ and sp² bonding characteristics, HREELS studies were performed in the aberration corrected STEM-FEI Titan 80–300 having an energy resolution of 0.15 eV. Fig. 3(b) shows a characteristic HREELS spectrum from the Q-carbon, which has a sloping edge at 285 eV with a broad peak at 292 eV. From the Voigt profile fit of the EELS spectrum, the sp³ was determined to be about 80% and the remaining 20% sp². These results on sp³/sp² ratio are consistent with the Raman spectrum, shown in Fig. 3(c), which shows a characteristic Q-carbon Raman spectrum containing both D and G peaks. From the fit to the Q-carbon spectrum, sp³ and sp² bonding fractions were estimated to be 80% and 20%, respectively.

The Q-carbon in the pure form shows robust coercivity and associated ferromagnetism at room temperature. From the variation of saturation magnetization with temperature, the Curie temperature was estimated to be over 650K. Fig. 4 shows M versus

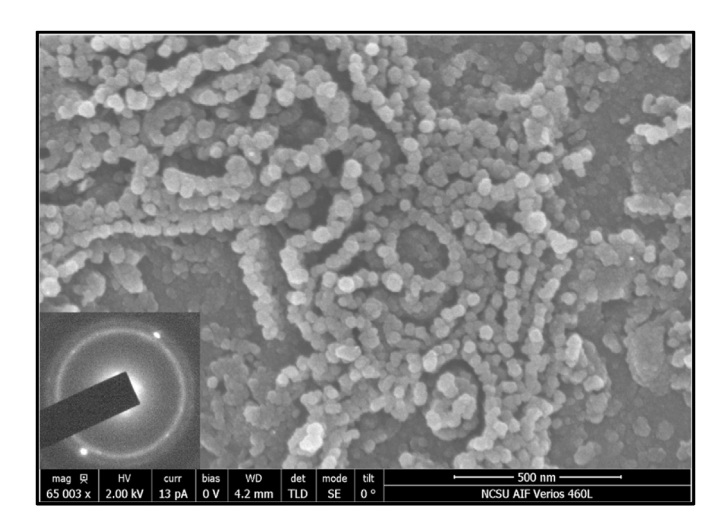


Fig. 2. High-resolution SEM showing formation of self-organized Q-carbon nanoballs along strings and rings with inset electron diffraction pattern from Q-carbon.

H plots before after laser annealing carbon layers. We investigated the effect of temperature on the coercivity and the saturation magnetization of Q-carbon nanoballs in the temperature range of 10–300K. Fig. 4 shows magnetic moment (M) versus field (H) plots at different temperatures 10K, 100K and 300K. The as-deposited films showed diamagnetic behavior of carbon before laser annealing. After laser annealing, we obtained a typical ferromagnetic loop with a robust coercivity of at different temperatures. The inset at a magnification shows coercivity of about 100 Oersteds at 300K. This value of coercivity at room temperature is quite adequate for drug coating and delivery applications.

The results on formation and characterization Q-BN balls are shown in Fig. 5. After melting amorphous BN layers (5-10 nm thick), the results are shown in Fig. 5 (a). These nanoballs (average size 60 nm) tend to form more in a stringlike (straight line) structure and less of circular ring structure, as observed for Q-carbon balls. The formation of strings occurs when BN tetrahedra align along <100> directions, as discussed later. Using high-resolution cross-section, these balls exhibit amorphous structure with inset showing diffraction pattern from (0001) sapphire substrate, as shown in Fig. 5(b). The amorphous structure of Q-BN is similar to that of Q-carbon (Fig. 3(a)). The amorphous Q-carbon and Q-BN structures are formed because of larger times needed for diamond and c-BN nucleation. The EELS spectrum from Q-BN (Fig. 5(c)) shows that Q-BN contains mostly sp³ bonding, unlike Q-carbon with 80% sp³ and 20% sp². However, it is found that the EELS spectrum of Q-BN has distinct features from h-BN and c-BN. The spectrum has B K-edge peaks at 195eV and 204eV corresponding to σ edges. The Q-BN has a higher sp³ fraction than h-BN but lower than that of c-BN which causes the above-mentioned shift in the $\boldsymbol{\sigma}$ edge peaks. There is an absence of sp² bonded (π^* peak) in Q-BN.

These bonding characteristics are reflected in magnetic properties, as Q-carbon is ferromagnetic, and Q-BN is diamagnetic. Theoretical calculations show that dangling bonds in Q-carbon associated with $\rm sp^3/sp^2$ interfaces are responsible for the magnetic moment and the ferromagnetism in Q-carbon [17]. The carbon dangling bonds with unpaired spins are located at the $\rm sp^3/sp^2$ interfaces. In the case of Q-BN, the bonding was determined to be mostly $\rm sp^3$, therefore, the number density of unpaired spins is expected to be very low. Thus, experimental results on diamagnetism and the absence of ferromagnetism in Q-BN are consistent with absence of $\rm sp^2$ bonded (π^* peak) in Q-BN.

4. Theoretical considerations

Following the linear thin-film hydrodynamic (TFH) instability framework [18], the characteristic spinodal wavelength (λ) during rapid quenching can be expressed as

$$(\lambda) = (16 \pi^3 \gamma / A)^{1/2} t^2 \dots \dots \dots (1)$$

where γ is the surface tension of carbon liquid, A is the Hamaker constant, and t is the layer thickness before instability.

Using the mass conservation, we obtain

$$(4/3) \pi D^{3} \rho_{q} = \lambda^{2} t \rho_{1} \dots \dots \dots \dots (2)$$

where D is the size of the nanoball, ρ_q is density of Q-carbon and ρ_l is the density of liquid carbon.

From equation (2), the size of nanoballs D can be expressed as

$$D = [(96 \pi^2 \gamma \rho_I)/(A \rho_0)]^{1/3} t^{5/3} \dots \dots \dots \dots (3)$$

Using the values for γ as 55 erg cm $^{-2}$, $A=4.69\times 10^{-12}$ erg and assuming $\rho_l=\rho_q$, we estimate D=60 nm for film thickness of 5 nm,

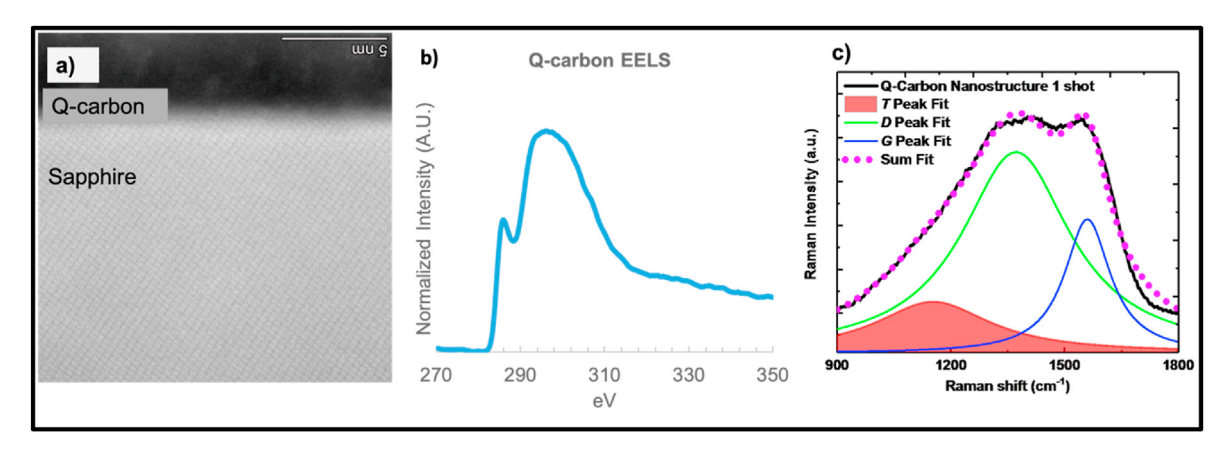


Fig. 3. (a) HRTEM cross-section showing amorphous Q-carbon on (0001) sapphire; (b) Electron-energy-loss spectrum (EELS) from Q-carbon with 80% sp³ and 20% sp², and (c) Raman spectrum from Q-carbon confirming with 80% sp³ and 20% sp². (A colour version of this figure can be viewed online.)

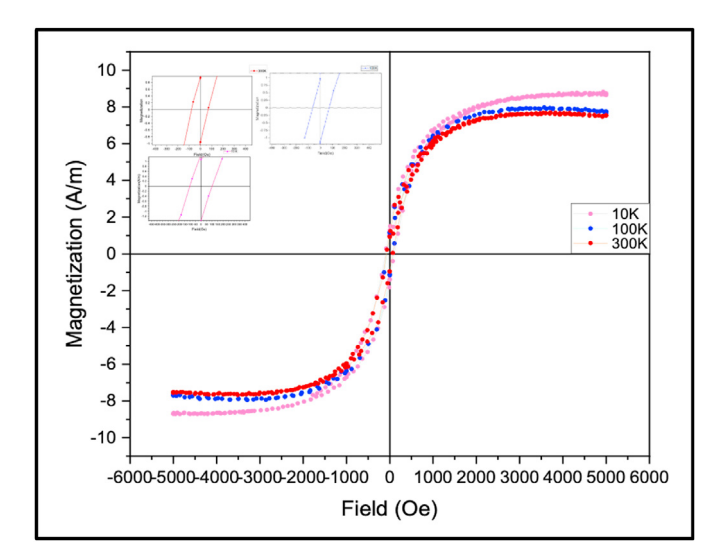


Fig. 4. Magnetic moment (M) versus field (H) plots for Q-carbon at various temperatures (300 K, 100 K and 10 K) with inset (bottom-right) showing the robust coercivity at 300 K. The as-deposited DLC at 300 K exhibited features diamagnetic nature. (A colour version of this figure can be viewed online.)

which is in good agreement with our experimental results.

The surface temperature versus time plots using SLIM calculations [4] for energy density ranging from 0.3 J cm⁻² to 0.6 J cm⁻² are displayed in Fig. 6(a). The temperature rise to 4000K is critical at which Q-carbon phase forms with undercooling of about 1000K. The temperature versus time profile is greatly affected by the sp³ to sp² ratio which affects photon energy absorption as well as thermal conductivity and heat dissipation during growth. To convert amorphous carbon films into diamond or Q-carbon phase, it is essential to first melt and then quench to induce first-order phase transformation. The heat flow is spatially and temporally confined, making it an ideal technique to study melting and quenching in materials, such as carbon and BN. The molten carbon is metallic with a thermal conductivity of 2.9 W/cm K. Hence, it can be quenched rapidly with cooling rates of 10^{10} – 10^{11} K/s. By varying the degree of undercooling, it is possible to achieve graphene, diamond, or Q-carbon phases. At critical PLA energy of 0.4 I/cm², the melting of amorphous carbon in the undercooled state is achieved. Fig. 6 (a) shows temperature as a function of time for different pulse energy densities, while keeping the laser pulse duration and laser wavelength the same. These results reveal that melting of carbon films on sapphire occurs as the film/substrate interface achieves temperature over 4000 K. As the nanosecond

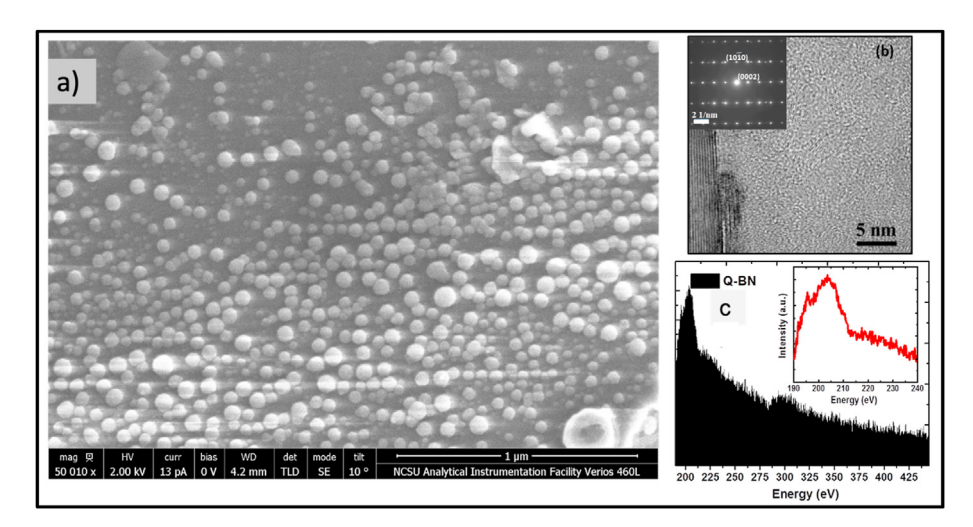


Fig. 5. (a) High-resolution SEM showing formation of self-organized Q-BN nanoballs along strings; (b) HRTEM cross-section showing amorphous Q-BN structure on sapphire (0001) with inset (-2110) diffraction pattern; and (c) characteristic Q-BN EELS showing 100% sp³ bonding.

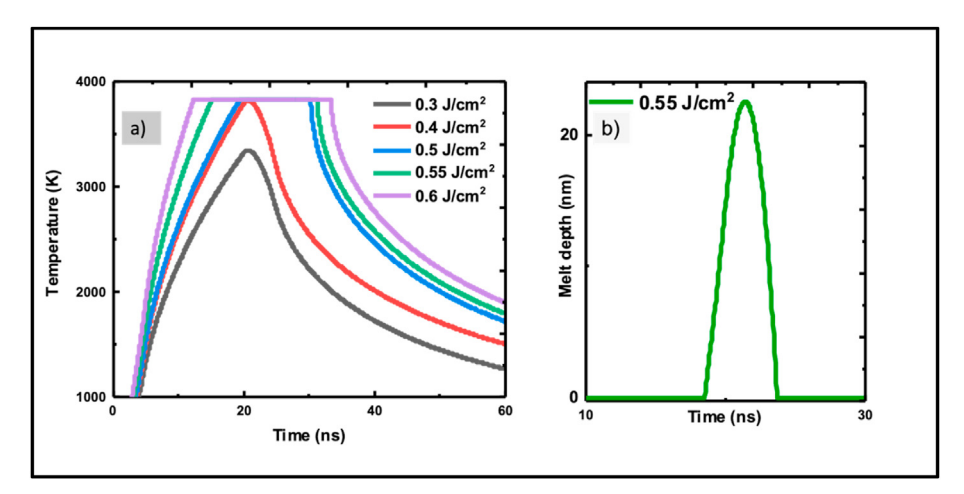


Fig. 6. SLIM calculations of temperature versus time during nanosecond laser annealing for different laser energy densities (0.3, 0.4, 0.5, 0.55, and 0.6 Jcm⁻²; and (b) Melt depth versus time for the 0.55Jcm⁻² laser pulse. (A colour version of this figure can be viewed online.)

laser pulse terminates, the melt front turns back to the surface. Fig. 6(b) shows melt depth versus time for 0.55 Jcm $^{-2}$ laser pulse. The diamond crystallites start growing as the laser pulse terminates and bends over, which leaves about 5ns for the growth of nanoballs. These nanoballs are formed in 20 nm wide region near the molten carbon and sapphire interface. The undercooling, ΔT_U , generates a pressure transient (dP/dt) with the rate of quenching (dT/dt). The change in pressure with time is related by dP/dt = (dP/dT)x(dT/dt) = -(ΔT_U , ΔH_m)/($T_m T \Delta V$)xdT/dt = -C $\Delta T_U x dT$ /dt, where C (ΔH_m /($T_m T \Delta V$)) remains fairly constant with ΔV as change in volume from liquid to solid. This equation directly relates the change in pressure with time and undercooling (ΔT_U) and the quenching rate (dT/dt), calculated from the SLIM program.

For ferromagnetic materials at low temperatures, the saturation magnetization, Ms as function of temperature is governed by the Bloch's law: $M_s(T) = M_s(0) [1 - (T/T_0)^{\alpha}]$, where $M_s(0)$ is the saturation magnetization at 0 K and To is the temperature at which the Ms (T) becomes zero, the same as Curie temperature [19]. From the saturation magnetization values as a function of temperature in Fig. 4, we obtained Curie temperature above 650K using Bloch's law. The Bloch's exponent α is 1.5 for bulk materials, which was derived by considering the magnon excitation of long-wavelength spin waves at low temperatures. However, in nanoballs with sizes smaller than wavelengths of magnons, we may induce a gap in the spin-wave energy spectrum [20]. At temperatures larger than the spin-wave energy gap, Bloch's law seems to be applicable in nanoballs, where the form remains the same and only the value of the exponent may differ from 1.5 ± 0.1 . Various interpretations have been proposed for the deviation from the Bloch's law in nanoparticles [20]. For example, the additional magnetization due to shell spins was suggested to induce the deviation from the Bloch law [21]. The deviation of the saturation magnetization from the Bloch law at temperatures below 50 K was suggested to be due to the canted surface spins which freeze into a disordered state [22]. The temperature dependence of coercivity $(H_C(T))$ is described by Kneller's law [23], where $H_C(T) = H_C(0) [1 - (T/T_C)^{\alpha}]$. Here T_C is the superparamagnetic blocking temperature of the nanoballs and H_C (0) is the coercivity at T = 0 K. Kneller law was derived in the temperature range (0 to T_c), where the nanoparticles were considered to be single-domain, non-interacting and with uniaxial anisotropy. For such systems, α was found be equal to $\frac{1}{2}$.

The formation of strings and rings in quenched carbon and Q-carbon is rationalized by the alignment of diamond tetrahedra along the <100> or <110> directions. The alignment in <100>

directions involves {100} planes, which can occur only in a straight line in <100> direction, as shown in Fig. 7(a). The inset shows three-dimensional arrangement of atoms between two adjacent tetrahedra. The <100> alignment leads to formation of strings, as observed in the case of Q-BN. On the other hand, the alignment in <110> direction involves <001> edges, which can bend (as shown in Fig. 7(b)) and form rings, as shown in Fig. 7(c). This pivoting of tetrahedra along <001> direction is key to formation of ring structure in Q-carbon. We envisage that the alignment of tetrahedra results from a dynamical heterogeneity, which has been studied experimentally and theoretically in supercooled liquids and spin glasses [24,25]. The formation of stringlike structure is found to increase with undercooling as we go to Q-carbon with the highest undercooling. These <110> strings (Fig. 7 (a)) can selforganize into rings to minimize line tension energy, as shown in Fig. 7(c). The diamond tetrahedra along these strings and rings provide critical nuclei for Q-phase formation. The size of the nanoballs along these rings is determined by the pulse duration and available time for growth in the liquid-phase during the quenching cycle. The nanodiamond ring structure is formed at a lower undercooling (as shown in our earlier studies [15]), with a smaller number density per unit length than those at Q-carbon undercooling, where nucleation density is much higher because of higher density of carbon tetrahedral packing.

The O-carbon structure consists of randomly packed diamond tetrahedra with packing efficiency >80%. The formation of Q-carbon has been confirmed theoretically [17,26] and experimentally [9] by other researchers. The diamond tetrahedra provide easy nucleation sites for Q-carbon growth. When three diamond tetrahedra get together in the form of a string (as in Q₁ phase), it may achieve a critical diamond nucleus for a homogeneous nucleation, estimated to be $\sim 1-2$ nm [27,28]. The Q₁ phase is formed when three diamond tetrahedra units are repeated randomly [9]. We have shown the formation of three distinct Q phases in B-doped Qcarbon (namely QB₁, QB₂, and QB₃) with superconducting transition temperature of 37K, 57K, and over 110K, respectively [9]. The hardness/stiffness and superconductivity are interrelated through $T_c = 0.2 (k/m)^{0.5}$, where T_c is the superconducting transition temperature, k is the spring constant, and m is the mass. Thus, the stiffer materials with light masses should have the highest superconducting transition temperature.

Magnetic properties, such as coercivity is zero at the superparamagnetic limit below a certain nanoball size, and then it increases with size attaining a maximum value and then decreasing

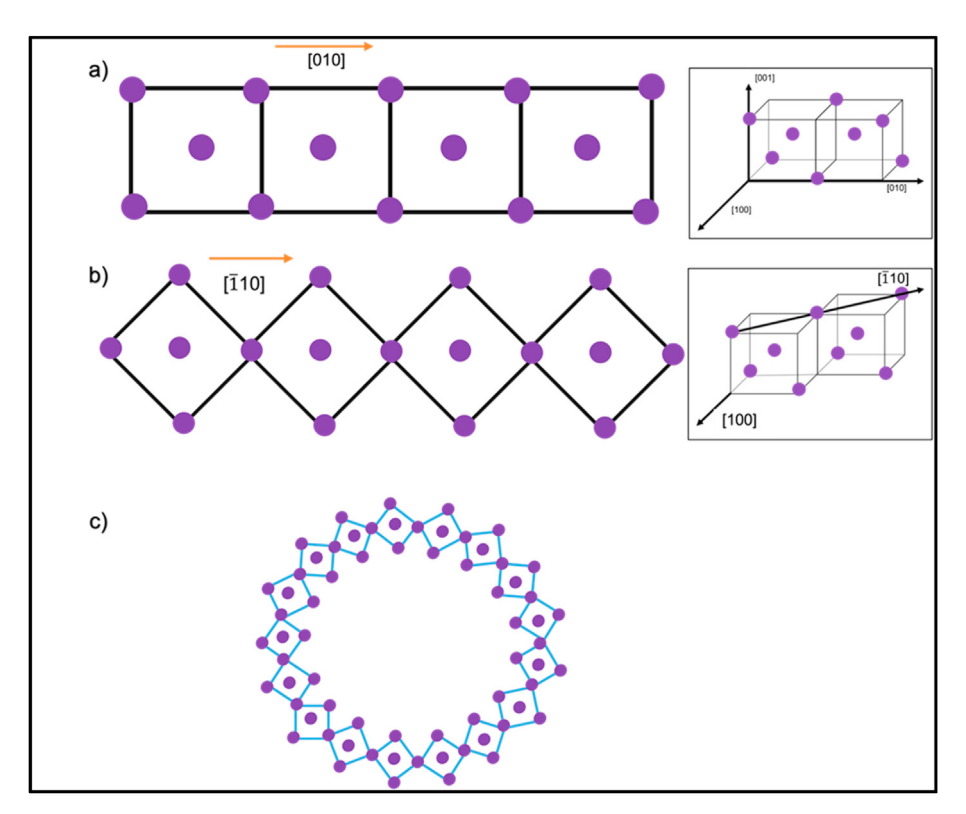


Fig. 7. (a) Schematic of alignment of diamond tetrahedra along the <100> direction for the formation of self-organized stringlike structures with inset showing detailed atomic arrangements; (b) alignment of diamond tetrahedra along the <110> direction for the formation of self-organized ring structures with inset showing detailed atomic arrangements; and (c) formation of self-organized ring structure from <110> alignment of tetrahedra. (A colour version of this figure can be viewed online.)

again. Thus, there is an optimum size for a maximum coercivity which is attained by manipulating thin film, laser and substrate variables. Similarly, there is a size effect on superconductivity and superconducting transition temperature (T_c). With decreasing size, the superconducting transition temperature in B-doped carbon nanoballs is envisaged to increase through a lowering of the phonon frequency (phonon softening), which results in an increase in the effective electron-phonon coupling, and hence the T_c for low to medium coupled superconductors. The decrease in the density of states due to quantization at lower sizes can reduce the superconducting transition temperature somewhat. Superconductivity occurs when a quantum condensate of paired electrons (Cooper pairs) is formed. In nanoparticles and other small particles, energy levels are quantized. Therefore, the average energy level spacing can exceed the superconducting energy gap, and it is at this point that superconductivity is believed to be affected adversely [29].

In summary, we have created nanoballs of O-carbon by melting carbon layers in the highly undercooled state and subsequent quenching at ambient pressure in air. Similarly, we formed Q-BN nanoballs by melting BN in the highly undercooled state and subsequent quenching at ambient pressure in air. These nanoballs can be self-organized in the form of strings and rings by aligning diamond tetrahedra along <100> and <110> directions, respectively. The size of these Q-carbon and Q-BN nanoballs can be varied from 5 to 100nm by manipulating laser, carbon film and substrate parameters. Pure and undoped Q-carbon films show robust ferromagnetism, and record BCS high-temperature superconductivity upon doping with boron. We expect B-doped Q-carbon nanoballs to have even higher superconducting transition temperature through stronger electron-phonon coupling. Earlier studies showed thin Qcarbon films to be harder than diamond as much 70%, therefore, nanoballs may be even harder than Q-carbon thin films [30]. The interaction between bacterial cells and carbon nanomaterials results in direct contact between the cells and carbon nanomaterials, which in turn leads to cell death. In view of these properties, ultrahard nanoballs are expected to find novel applications ranging from targeted drug delivery and biomedical applications to nanosensing and highly efficient field-emission displays [31].

CRediT authorship contribution statement

J. Narayan: Conceptualization, Funding acquisition, and some experimental work. **N. Khosla:** Methodology, experimental work, and, Formal analysis.

Declaration of competing interest

The authors declare that they have no known competing financial interests or personal relationships that could have appeared to influence the work reported in this paper.

Acknowledgement

This work was supported by the National Science Foundation Grant (DMR-2016256). The comments and discussions with Professor John Prater are gratefully acknowledged.

References

- [1] F.P. Bundy, W.A. Bassett, M.S. Weathers, R.J. Hemley, H.U. Mao, A.F. Goncharov, The pressure-temperature phase and transformation diagram for carbon; updated through 1994, Carbon 34 (2) (1996) 141–153, https://doi.org/ 10.1016/0008-6223(96)00170-4.
- J.C. Angus, C.C. Hayman, Science241, 913 (1988) and JC angus, in: Proc. Of Symposium on Diamond and Diamond-like Materials, 1989, https://doi.org/ 10.1126/science.241.4868.913.

[3] X. Chen, J. Narayan, Effect of the chemical nature of transition-metal substrates on chemical-vapor deposition of diamond, J. Appl. Phys. 74 (6) (1993) 4168–4173, https://doi.org/10.1063/1.354420.

- [4] R.K. Singh, D.R. Gilbert, J. Fitz-Gerald, S. Harkness, D.G. Lee, Engineered interfaces for adherent diamond coatings on large thermal-expansion coefficient mismatched substrates, Science 272 (1996) 396–398, https://doi.org/10.1126/science.272.5260.396, 5260.
- [5] D. Das, R.N. Singh, A review of nucleation, growth and low temperature synthesis of diamond thin films, Int. Mater. Rev. 52 (1) (2007) 29–64, https:// doi.org/10.1179/174328007X160245.
- [6] J. Narayan, A. Bhaumik, Novel phase of carbon, ferromagnetism, and conversion into diamond, J. Appl. Phys. 118 (2015), https://doi.org/10.1063/1.4936595, 215303, 21.
- [7] J. Narayan, A. Bhaumik, W. Xu, Direct conversion of h-BN into c-BN and formation of epitaxial c-BN/diamond heterostructures, J. Appl. Phys. 119 (2016), https://doi.org/10.1063/1.4948688, 185302, 18.
- [8] J. Narayan, A. Bhaumik, S. Gupta, A. Haque, R. Sachan, Progress in Q-carbon and related materials with extraordinary properties, Mater. Res. Lett. 6 (7) (2018) 353–364, https://doi.org/10.1080/21663831.2018.1458753.
- [9] J. Narayan, A. Bhaumik, R. Sachan, High temperature superconductivity in distinct phases of amorphous B-doped Q-carbon, J. Appl. Phys. 123 (13) (2018) 135304. https://doi.org/10.1063/1.5016397.
- [10] A. Bhaumik, J. Narayan, Structure—property correlations in phase-pure B-doped Q-carbon high-temperature superconductor with a record T c= 55 K, Nanoscale 11 (18) (2019) 9141–9154, https://doi.org/10.1039/C9NR00562E.
- [11] R. Sachan, J.A. Hachtel, A. Bhaumik, A. Moatti, J. Prater, J.C. Idrobo, J. Narayan, Emergence of shallow energy levels in B-doped Q-carbon: a high-temperature superconductor, Acta Mater. 174 (2019) 153–159, https://doi.org/10.1016/iactamat 2019.05.013
- [12] Y. Hiroki, S. Inubushi, T. Wakita, T. Yokoya, Y. Muraoka, Formation of Q-carbon by adjusting sp3 content in diamond-like carbon films and laser energy density of pulsed laser annealing, Carbon 167 (2020) 504–511, https:// doi.org/10.1016/j.carbon.2020.06.025.
- [13] J. Narayan, A. Bhaumik, S. Gupta, P. Joshi, P. Riley, R.J. Narayan, Role of Q-carbon in nucleation and formation of continuous diamond film, Carbon 176 (2021) 558–568, https://doi.org/10.1016/j.carbon.2021.02.049.
- [14] R.K. Singh, J. Narayan, A novel method for simulating laser-solid interactions in semiconductors and layered structures, Mater. Sci. Eng., B 3 (3) (1989) 217–230, https://doi.org/10.1016/0921-5107(89)90014-7.
- [15] J. Narayan, A. Bhaumik, S. Gupta, P. Joshi, P. Riley, R.J. Narayan, Formation of self-organized nano-and micro-diamond rings, Mater. Res. Lett. 9 (7) (2021) 300–307, https://doi.org/10.1080/21663831.2021.1907627.
- [16] J. Narayan, P. Joshi, J. Smith, W. Gao, W.J. Weber, R.J. Narayan, Q-carbon as a new radiation-resistant material, Carbon 186 (2022) 253–261, https:// doi.org/10.1016/j.carbon.2021.10.006.
- [17] S. Yuki, J.R. Chelikowsky, M.L. Cohen, Magnetism in amorphous carbon, Phys.

- Rev. Mater. 2 (7) (2018), 074403, https://link.aps.org/doi/10.1103/ PhysRevMaterials.2.074403.
- [18] T. Justin, D. Thomas, C. Favazza, R. Sureshkumar, R. Kalyanaraman, Pulsed-laser-induced dewetting in nanoscopic metal films: theory and experiments, Phys. Rev. B 75 (2007). https://link.aps.org/doi/10.1103/PhysRevB.75.235439, 235439, 23.
- [19] Felix Bloch, On the theory of ferromagnetism, Z. Phys. 61 (3-4) (1930) 206-219.
- [20] K. Maaz, A. Mumtaz, S.K. Hasanain, M.F. Bertino, Temperature dependent coercivity and magnetization of nickel ferrite nanoparticles, J. Magn. Magn Mater. 322 (15) (2010) 2199–2202, https://doi.org/10.1016/ i.immm.2010.02.010.
- [21] L.D. Tung, V. Kolesnichenko, D. Caruntu, N.H. Chou, C.J. O'connor, L. Spinu, Magnetic properties of ultrafine cobalt ferrite particles, J. Appl. Phys. 93 (10) (2003) 7486–7488, https://doi.org/10.1063/1.1540145.
- [22] C.R. Alves, R. Aquino, J. Depeyrot, T.A.P. Cotta, M.H. Sousa, F.A. Tourinho, H.R. Rechenberg, G.F. Goya, Surface spin freezing of ferrite nanoparticles evidenced by magnetization measurements, J. Appl. Phys. 99 (8) (2006), https://doi.org/10.1063/1.2163844, 08M905.
- [23] X. Batlle, M. Garcia del Muro, J. Tejada, H. Pfeiffer, P. Görnert, E. Sinn, Magnetic study of M-type doped barium ferrite nanocrystalline powders, J. Appl. Phys. 74 (5) (1993) 3333–3340, https://doi.org/10.1063/1.354558.
- [24] D. Claudio, J.F. Douglas, W. Kob, S.J. Plimpton, P.H. Poole, S.C. Glotzer, Stringlike cooperative motion in a supercooled liquid, Phys. Rev. Lett. 80 (1998), https://doi.org/10.1103/PhysRevLett.80.2338, 2338, 11.
 [25] Y. Gebremichael, M. Vogel, S.C. Glotzer, Particle dynamics and the develop-
- ment of string-like motion in a simulated monoatomic supercooled liquid, J. Chem. Phys. 120 (9) (2004) 4415–4427, https://doi.org/10.1063/1.1644539.
- [26] S. Yuki, J.R. Chelikowsky, M.L. Cohen, Simulating the effect of boron doping in superconducting carbon, Phys. Rev. B 97 (2018) 5, 054501, https://link.aps. org/doi/10.1103/PhysRevB.97.054501.
- [27] R.F. Wood, D.H. Lowndes, J. Narayan, Bulk nucleation and amorphous phase formation in highly undercooled molten silicon, Appl. Phys. Lett. 44 (8) (1984) 770–772, https://doi.org/10.1063/1.94912.
- [28] D.H. Lowndes, R.F. Wood, J. Narayan, Pulsed-laser melting of amorphous silicon: time-resolved measurements and model calculations, Phys. Rev. Lett. 52 (1984). https://link.aps.org/doi/10.1103/PhysRevLett.52.561, 561, 7.
- [29] S. Bosé, P. Raychaudhuri, R. Banerjee, P. Vasa, P. Ayyub, Mechanism of the size dependence of the superconducting transition of nanostructured Nb, Phys. Rev. Lett. 95 (2005). https://link.aps.org/doi/10.1103/PhysRevLett.95.147003, 147003, 14.
- [30] J. Narayan, S. Gupta, A. Bhaumik, R. Sachan, F. Cellini, E. Riedo, Q-carbon harder than diamond, MRS Commun. 8 (2018) 428.
- [31] P.R. Riley, R.J. Narayan, Recent advances in carbon nanomaterials for biomedical applications: a Review, Curr. Opin. Biomed. Eng. 17 (2021) 100262, https://doi.org/10.1016/J.COBME.2021.100262.